

Algorithmic depth compensation improves quantification and noise suppression in functional diffuse optical tomography

Fenghua Tian, Haijing Niu, Sabin Khadka, Zi-Jing Lin, and Hanli Liu*

Department of Bioengineering, the University of Texas at Arlington, 501 West First Street, Arlington, TX 76019, USA

*hanli@uta.edu

Abstract: Accurate depth localization and quantitative recovery of a regional activation are the major challenges in functional diffuse optical tomography (DOT). The photon density drops severely with increased depth, for which conventional DOT reconstruction yields poor depth localization and quantitative recovery. Recently we have developed a depth compensation algorithm (DCA) to improve the depth localization in DOT. In this paper, we present an approach based on the depth-compensated reconstruction to improve the quantification in DOT by forming a spatial prior. Simulative experiments are conducted to demonstrate the usefulness of this approach. Moreover, noise suppression is a key to success in DOT which also affects the depth localization and quantification. We present quantitative analysis and comparison on noise suppression in DOT with and without depth compensation. The study reveals that appropriate combination of depth-compensated reconstruction with the spatial prior can provide accurate depth localization and improved quantification at variable noise levels.

©2010 Optical Society of America

OCIS codes: (170.2655) Functional monitoring and imaging; (170.3010) Image reconstruction techniques; (170.6960) Tomography.

References and links

1. A. Villringer, and B. Chance, "Non-invasive optical spectroscopy and imaging of human brain function," *Trends Neurosci.* **20**(10), 435–442 (1997).
 2. D. A. Boas, A. M. Dale, and M. A. Franceschini, "Diffuse optical imaging of brain activation: approaches to optimizing image sensitivity, resolution, and accuracy," *Neuroimage* **23**(Suppl 1), S275–S288 (2004).
 3. C. K. Lee, C. W. Sun, P. L. Lee, H. C. Lee, C. Yang, C. P. Jiang, Y. P. Tong, T. C. Yeh, and J. C. Hsieh, "Study of photon migration with various source-detector separations in near-infrared spectroscopic brain imaging based on three-dimensional Monte Carlo modeling," *Opt. Express* **13**(21), 8339–8348 (2005).
 4. R. Arridge, "Optical tomography in medical imaging," *Inverse Probl.* **15**(2), R41–R93 (1999).
 5. H. Niu, F. Tian, Z. J. Lin, and H. Liu, "Development of a compensation algorithm for accurate depth localization in diffuse optical tomography," *Opt. Lett.* **35**(3), 429–431 (2010).
 6. H. Niu, Z. Lin, F. Tian, S. Dhamne, and H. Liu, "Comprehensive Investigation of three-dimensional diffuse optical tomography with depth compensation algorithm," *J. Biomed. Opt.* in press.
 7. M. Cope, D. T. Delpy, E. O. Reynolds, S. Wray, J. Wyatt, and P. van der Zee, "Methods of quantitating cerebral near infrared spectroscopy data," *Adv. Exp. Med. Biol.* **222**, 183–189 (1988).
 8. H. Dehghani, B. W. Pogue, J. Shudong, B. Brooksby, and K. D. Paulsen, "Three-dimensional optical tomography: resolution in small-object imaging," *Appl. Opt.* **42**(16), 3117–3128 (2003).
 9. G. Boverman, E. L. Miller, A. Li, Q. Zhang, T. Chaves, D. H. Brooks, and D. A. Boas, "Quantitative spectroscopic diffuse optical tomography of the breast guided by imperfect a priori structural information," *Phys. Med. Biol.* **50**(17), 3941–3956 (2005).
 10. E. R. Hom, <http://www.nmr.mgh.harvard.edu/PMI/toolbox/index.html>
 11. L. Wu, "A parameter choice method for Tikhonov regularization," *Electron. Trans. Numer. Anal.* **16**, 107–128 (2003).
 12. P. C. Hansen, and D. O'Leary, "The use of the L-curve in the regularization of discrete ill-posed problems," *SIAM J. Sci. Comput. (USA)* **14**(6), 1487–1503 (1993).
 13. B. W. Zeff, B. R. White, H. Dehghani, B. L. Schlaggar, and J. P. Culver, "Retinotopic mapping of adult human visual cortex with high-density diffuse optical tomography," *Proc. Natl. Acad. Sci. U.S.A.* **104**(29), 12169–12174 (2007).
-

1. Introduction

In the past decade, diffuse optical tomography (DOT) has become a promising technique to image functional brain activities [1,2] while being non-invasive, portable and biologically safe. Given the size and contour of the human head, reflectance geometry is widely used with the sources and detectors placed on the same side of the head and a few centimeters apart. However, the photon density in reflectance geometry drops rapidly with increased depth in tissue [3], i.e., deep absorption perturbation has low contribution to the intensity change measured on the surface. It follows that the sensitivity matrix, \mathbf{A} , is ill-posed along depth. In conventional DOT reconstruction algorithm using Tikhonov regularization [2,4], the ill-posed \mathbf{A} matrix results in a significant error in depth localization [2]. Since the magnitude of reflectance measurement is highly sensitive to the depth of local absorption perturbation, it becomes unrealistic to accurately quantify the local absorption perturbation without knowing its actual depth.

Recently we have developed a depth compensation algorithm (DCA) [5] to improve the accuracy of depth localization in three-dimensional (3D) DOT. It introduces a weight matrix, \mathbf{M} , to counterbalance the severe sensitivity decay of \mathbf{A} matrix along depth. The original \mathbf{A} matrix is replaced by a depth-compensated matrix, \mathbf{AM} , in reconstruction. The improved accuracy in depth localization by the depth compensation algorithm has been demonstrated in both laboratory phantom experiments and *in vivo* human brain study [6]. Thus, it is expected that this algorithm will also improve the quantification in DOT with a reasonable accuracy. However, this improvement cannot be achieved directly. It is because the matrix \mathbf{AM} used in depth-compensated reconstruction is not in compliance with the actual measurement. Although the reconstructed image with depth compensation can reflect the actual location and size of local absorption perturbation, the quantity of the image does not reflect the actual quantity of the absorption perturbation. Thus, it is necessary to further develop an approach, which is based on the depth-compensated reconstruction, to improve the quantification in DOT. In this paper, we present such an approach which improves the quantification of local absorption perturbation by forming a spatial constraint or prior in reconstructed image. Simulative experiments are conducted to confirm the usefulness of this approach.

Moreover, in real measurement the data will inevitably contain noise which can be instrumental, physiological [2] or both. Mathematically, a parameter α is used in Tikhonov regularization to stabilize and optimize the solution of an ill-posed inverse problem [4] which suppresses the noise. Noise suppression is a key to success in DOT. However, it also affects the depth localization and quantification. For example, a set of real measurement data with a higher noise level will require a bigger regularization parameter in reconstruction, which may suppress more subtle but true signals that are likely to stem from deep tissues and consequently results in a bigger localization error in depth. In this paper, thus, we will also offer comparative analysis on noise suppression in DOT without and with the use of depth compensation.

2. Methods

2.1 Reconstruction and depth compensation

The measurement of absorption perturbation in a turbid medium is based on the modified Beer-Lambert law [7]. For a 3D medium, it can be generalized as [2]:

$$\Delta OD(\lambda, t) = \sum_{j=1}^{N_{\text{vox}}} \Delta \mu_{a,j}(\lambda, t) L_j(\lambda) \quad (1)$$

where $\Delta OD(\lambda, t)$ is the change in optical density (OD) attained from a source-detector pair (measurement) at wavelength λ and time t , $\Delta \mu_{a,j}$ is the absorption perturbation in the j th voxel of the medium, and L_j is the effective path length of detected photons through the j th voxel.

In DOT, multiple measurements are used to reconstruct an image of absorption perturbation. Thus, Eq. (1) can be written in a matrix/vector form as (hereafter we will omit variables λ and t):

$$\mathbf{y} = \mathbf{A}\mathbf{x} \quad (2)$$

where \mathbf{y} denotes the vector of ΔOD_i ($i = 1 \dots N_{meas}$) from all the measurements, \mathbf{x} denotes the vector of $\Delta\mu_{a,j}$ ($j = 1 \dots N_{vox}$) from all the voxels in the 3D medium, and \mathbf{A} is a $N_{meas} \times N_{vox}$ sensitivity matrix of $L_{i,j}$ and can be derived from the photon diffusion equation using the Rytov approximation [4]. In conventional DOT, the inverse solution of Eq. (2) is given based on Tikhonov regularization [2]:

$$\hat{\mathbf{x}}_{DOT} = \mathbf{A}^T (\mathbf{A}\mathbf{A}^T + \alpha s_{\max} \mathbf{I})^{-1} \mathbf{y} \quad (3)$$

where \mathbf{I} is the identity matrix, s_{\max} is the maximum eigen-value of $\mathbf{A}\mathbf{A}^T$, and α is the regularization parameter to stabilize the solution and to suppress the noise existing in a real measurement.

However, in matrix \mathbf{A} the elements from superficial layers are significantly greater in magnitude than those from deeper layers due to severe attenuation in photon density with increased depth. In depth-compensated reconstruction, a weight matrix, \mathbf{M} , is created appropriately [5] and multiplied to matrix \mathbf{A} in order to counterbalance the severe decay along depth. Specifically, the maximum singular value of layered sub-matrix \mathbf{A}_k ($k = 1 \dots N_{layer}$), denoted by $s_{\max,k}$ for the k th depth, is inversely arranged to form matrix \mathbf{M} :

$$\mathbf{M} = \begin{bmatrix} s_{\max, N_{layer}} \mathbf{I} & & & \\ & s_{\max, N_{layer}-1} \mathbf{I} & & \\ & & \dots & \\ & & & s_{\max, 1} \mathbf{I} \end{bmatrix}^{\gamma} \quad (4)$$

where power γ is the parameter to adjust the weight of \mathbf{M} . An optimal value of γ exists and has been determined empirically [5,6] with a range of 1.0 to 1.6. Then the depth-compensated matrix $\mathbf{A}^{\#} = \mathbf{A}\mathbf{M}$ is used to replace the actual sensitivity matrix \mathbf{A} in Eq. (3), leading to

$$\hat{\mathbf{x}}_{DCA} = (\mathbf{A}\mathbf{M})^T [(\mathbf{A}\mathbf{M})(\mathbf{A}\mathbf{M})^T + \alpha s'_{\max} \mathbf{I}]^{-1} \mathbf{y} \quad (5)$$

where s'_{\max} is the maximum eigen-value of $(\mathbf{A}\mathbf{M})(\mathbf{A}\mathbf{M})^T$.

2.2 Quantification approach based on depth-compensated reconstruction

We have developed an approach in order to quantify the absorption perturbation based on the reconstructed image with depth compensation. This approach has two steps: the first step is to determine a scaling parameter that will remove the artificial factor induced by matrix \mathbf{M} ; the second step is to define an appropriate region of interest (ROI) in the reconstructed image to form a spatial hard prior or constraint.

(1) *Determination of scaling parameter:* By introducing the weight matrix \mathbf{M} , the depth compensation algorithm actually derives the solution from an artificial forward model $\mathbf{y} = \mathbf{A}\mathbf{M}\hat{\mathbf{x}}_{DCA}$. Since the depth-compensated reconstruction has been demonstrated to retrieve the actual size and location of local absorption perturbation within experiment error [5,6], we assume the depth-compensated solution, $\hat{\mathbf{x}}_{DCA}$, can be applied to the original forward problem by introducing an scaling parameter K . Thus, Eq. (2) can be rewritten as:

$$\mathbf{y} = K\mathbf{A}\hat{\mathbf{x}}_{DCA} \quad (6)$$

where \mathbf{y} is attained from actual measurements, \mathbf{A} is the original sensitivity matrix and can be obtained through the calculation of forward problem, $\hat{\mathbf{x}}_{DCA}$ is the reconstructed image from Eq.

(5), and only K is unknown and can be solved in principle. In this paper the optimal estimation of K is carried out by linear regression across all the measurements. After K value is determined, $\hat{\mathbf{x}}'_{DCA} = K\hat{\mathbf{x}}_{DCA}$ becomes a new solution of depth-compensated reconstruction with correct scale. In this paper, all the reconstructed images with depth compensation to be shown are from $\hat{\mathbf{x}}'_{DCA}$.

(2) *Formation of spatial prior*: A general problem in DOT is the poor spatial resolution, which is partially attributed to the diffuse nature of photons and partially attributed to the limited number of measurements as compared to the huge number of voxels to be quantified in the medium. As a result, the outline of the absorber is blurred, and the recovered quantities of absorption perturbation are reduced in the reconstructed DOT image. A widely used approach to improve such a problem is to combine DOT with a spatial prior or constraint of abnormal structures that can be obtained from other high-resolution imaging modalities, such as CT and MRI [8,9]. However, independent usage of DOT as a stand-alone unit will be reduced by using this approach.

Since the depth compensation algorithm is able to determine the accurate location and size of local absorption perturbation, it may allow us to form a spatial prior directly from the reconstructed image, rather than from other imaging modalities, to quantify the values of local absorption perturbation with reasonable accuracy. Specifically, we first identify a ROI in the reconstructed images by applying a half-maximum threshold (or a half-minimum threshold for globally negative absorption perturbation). The identified ROI is then used to form a spatial hard prior with two assumptions: (1) the absorption perturbation in the medium originates from only the identified ROI and is negligible beyond this ROI, and (2) the absorption perturbation is homogeneous within the ROI, denoted by $\Delta\mu_{a_ROI}$. Based on these assumptions, Eq. (2) after the spatial prior is applied can be rewritten as:

$$\mathbf{y} = \Delta\mu_{a_ROI} \sum_{j \in ROI} L_{i,j} \quad (7)$$

In Eq. (7) the only unknown parameter is $\Delta\mu_{a_ROI}$. The optimal estimation of $\Delta\mu_{a_ROI}$ is then determined via linear regression across all measurements.

2.3 Simulative experiments

Three simulative experiments were conducted to validate our new quantification approach using a Photon Migration Imaging (PMI) toolbox available online [10]. The homogeneous medium had absorption and reduced scattering coefficients of 0.1 and 10 cm⁻¹, respectively. A 5 × 5 optode array (13 sources and 12 detectors) with an interval of 1.4 cm was arranged on the surface of medium, producing 132 measurements when the 1st to 4th nearest source-detector pairs were used (separation ranged from 1.4 to 5.0 cm). No noise was added to the data during the calculation of forward problem. In accordance with the coordinate system shown in Figs. 1(a) to 1(c), images of absorption perturbation were reconstructed in a 3D volume under the probe with $x = -3$ to 3 cm, $y = -3$ to 3 cm and $z = -0.4$ to -3 cm. The voxel size was 0.1 × 0.1 × 0.1 cm³. In each experiment, one (or two) cylindrical absorber(s) was (were) embedded into the medium with one circular side facing up to mimic the absorption perturbation due to brain activation(s). The absorber(s) had an identical diameter of 1.6 cm and thickness of 0.8 cm. The reduced scattering coefficient of the absorber(s) was the same as the background medium.

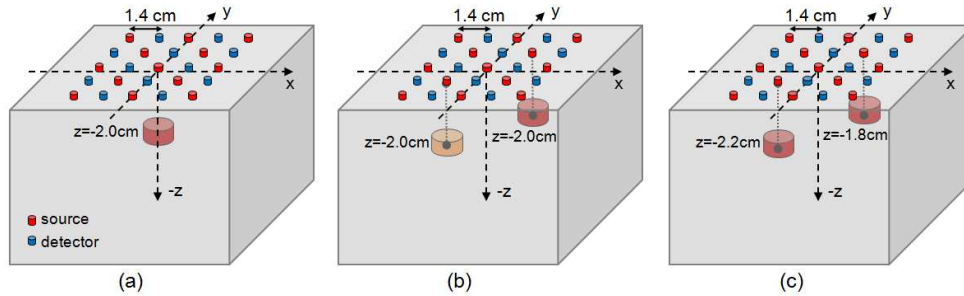


Fig. 1. Setups of simulative experiments: (a) experiment I, (b) experiment II, and (c) experiment III.

In experiment I, one cylindrical absorber was located right under the center of the optode array at a depth of $z = -2$ cm, as shown in Fig. 1(a). The absorption coefficient of the absorber was 0.3 cm^{-1} (i.e., the actual perturbation due to the presence of the absorber, $\Delta\mu_a$, is 0.2 cm^{-1}).

In experiment II, two cylindrical absorbers with different absorption coefficients were used to mimic brain activations occurring simultaneously at two different locations. As shown in Fig. 1(b), two absorbers were located along one diagonal direction ($y = x$) of the optode array with a separation of 4.2 cm in lateral span (x - y plane). Both of them were located at a depth of $z = -2$ cm. One absorber had an absorption coefficient of 0.2 cm^{-1} and the other one was 0.3 cm^{-1} .

In experiment III, two cylindrical absorbers with same absorption coefficient were located at two different depths. As shown in Fig. 1(c), two absorbers were located along one diagonal direction ($y = x$) of the optode array with a separation of 4.2 cm in lateral span. One absorber was at a depth of $z = -2.2$ cm and the other one was at $z = -1.8$ cm. Both absorbers had the same absorption coefficient of 0.3 cm^{-1} .

For all the simulative experiments, first images of the cylindrical absorber(s) were reconstructed with depth compensation. As mentioned in Section 2.1, the optimal value of γ ranges from 1.0 to 1.6. In this study a medium γ value of 1.3 was used. Although no noise was added in the forward simulation, we used $\alpha = 10^{-3}$ in regularization which was a representative value we had used in tissue-like phantom experiments. To evaluate the quantification accuracy of the reconstructed image, we used two parameters: the first parameter was the maximum absorption perturbation, $\Delta\mu_{a,max}$, in the scale-corrected image (i.e., $\hat{\mathbf{x}}'_{DCA}$) without any spatial prior. The second parameter was the quantified absorption perturbation with spatial prior, $\Delta\mu_{a,ROI}$.

Second, similar image reconstruction ($\alpha = 10^{-3}$) and evaluation process was repeated using the conventional DOT reconstruction algorithm [2] without depth compensation. In this way, a comparison between the results with and without depth compensation was made for each experiment.

2.4 Noise suppression

The regularization parameter, α , seen in Eqs. (3) and (5) is used to suppress the noise existing in real measurements. The optimal α value for DOT is usually determined by an L-curve algorithm [11,12]. In general, a bigger α value has to be used for data with a higher noise level to suppress the noise more severely. However, a bigger α simultaneously suppresses more subtle but true signals that are likely to stem from deep tissues and consequently results in a bigger localization error in depth. When the depth compensation algorithm is applied, this suppression becomes more complex since another parameter, γ , is introduced to adjust the power of depth compensation. These two parameters may have interaction or crosstalk. Based on the setup of simulative experiment I, which is shown in Fig. 1(a), we investigated the potential interaction between α and γ in the following three aspects:

Noise interference: Two data sets were generated when calculating the forward problem: the first data set was noise-free and the second one was added with 1% random noise. For both data sets, images of the absorber were reconstructed with and without depth compensation, respectively. In each reconstructed image the location of voxel with maximum absorption perturbation was identified to represent the central location of the absorber. Since the regularization parameter α was responsible for noise suppression, we altered the α value in reconstruction from 1 to 10^{-6} at a logarithm step size of 10^{-1} ($1, 10^{-1}, 10^{-2}, \dots, 10^{-6}$) and then compared the results from data with and without random noise. In this way, the sensitivity of respective reconstruction algorithm (with or without depth compensation) to noise can be seen clearly.

Depth localization: For depth-compensated reconstruction, we varied the γ value from 1.1, 1.3 to 1.5 simultaneously while modifying α values to investigate if γ had any cross effect with α on depth localization. It is noteworthy that the conventional DOT algorithm without depth compensation is equivalent to the case of $\gamma = 0$ when depth compensation is applied. For each pair of α and γ , the location of the reconstructed absorber was again represented by the location of voxel with maximum value of absorption perturbation.

Quantification: Using the data set with 1% random noise, values of $\Delta\mu_{a_max}$ and $\Delta\mu_{a_ROI}$ of the absorber were also quantified from the reconstructed images at variable α and γ values, and then compared between reconstruction algorithms with and without depth compensation.

3. Results

3.1 Reconstruction and quantification

Experiment I: Figs. 2(a) to 2(c) show depth cross sections (y-z plane, $x = 0$) of the actual absorber, the reconstructed DOT images without and with depth compensation from the simulation setup shown in Fig. 1(a). The reconstructed image without depth compensation has a significant localization error in depth. Its maximum value, $\Delta\mu_{a_max}$, is 0.059 cm^{-1} and located at about $z = -1.4 \text{ cm}$, as seen in Fig. 1(b). By applying the half-maximum threshold, the recovered absorption perturbation within ROI, $\Delta\mu_{a_ROI}$, remains to be 0.059 cm^{-1} , which is about 30% of the actual value. After using depth compensation but without spatial prior, the reconstructed image recovers $\Delta\mu_{a_max}$ to be 0.070 cm^{-1} and locates at $z = -1.9 \text{ cm}$, as shown in Fig. 1(c). If half-maximum thresholding is utilized to define ROI as a spatial prior, the recovered absorption perturbation with depth-compensated reconstruction is dramatically improved to be 0.122 cm^{-1} , about 61% of the actual value. It is mainly because the identified ROI in reconstructed image with depth compensation can retrieve the location and size of the actual absorber very well, as illustrated by the dash circle in Fig. 3(c).

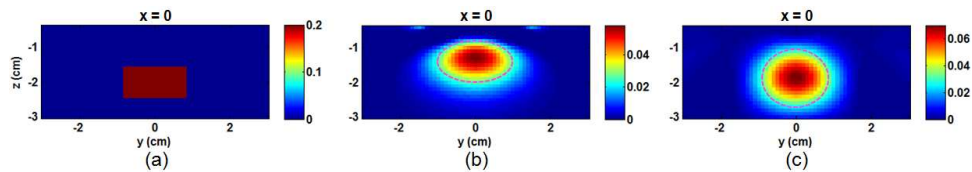


Fig. 2. For experiment I, a depth cross section (y-z plane, $x = 0$) of the (a) actual absorber, (b) reconstructed DOT image without depth compensation, and (c) reconstructed DOT image with depth compensation. The dash circles in (b) and (c) mark the ROIs with half-maximum threshold.

Experiment II: Figs. 3(a) and 3(b) show a depth cross section along the diagonal plane at $y = x$ [shown by the dashed line in Fig. 3(b)] and a lateral cross section in the x-y plane at $z = -2.0 \text{ cm}$ for the two simulated absorbers [see Fig. 1(b)], respectively. Both absorbers are at $z = -2.0 \text{ cm}$. The actual $\Delta\mu_a$ values of the two absorbers are 0.1 and 0.2 cm^{-1} , respectively. Correspondingly, Figs. 3(c) and 3(d) show the depth and lateral cross sections of the reconstructed DOT images without depth compensation. Both of the absorbers are untruthfully projected to a depth of $z = -1.4 \text{ cm}$. Therefore, $z = -1.4 \text{ cm}$ was chosen to plot

the lateral cross section, as shown in Fig. 3(d). Without either depth compensation or spatial prior applied, the $\Delta\mu_{a_max}$ values for the two absorbers are 0.024 and 0.048 cm^{-1} , about 24% of the actual values. In this case since the two absorbers can be clearly separated in the reconstructed images, two individual ROIs are identified in two sub regions using their respective half-maxima. The determined $\Delta\mu_{a_ROI}$ values for the two absorbers are 0.022 and 0.048 cm^{-1} , as low as the $\Delta\mu_{a_max}$ values.

At last, Figs. 3(e) and 3(f) show the depth and lateral cross sections of the reconstructed DOT images with depth compensation. The two absorbers are projected to $z = -1.9$ cm, which is very close to their actual locations. Therefore, the x-y lateral cross section is drawn at $z = -1.9$ cm, as given in Fig. 3(f). With depth compensation being applied but without ROI-based spatial prior, the recovered $\Delta\mu_{a_max}$ values for the two absorbers are 0.027 and 0.058 cm^{-1} , having a recovery rate of 27-29% of the actual values. Then, after two sub ROIs (described above) are appropriately identified, the reconstructed values of $\Delta\mu_{a_ROI}$ for the two absorbers are improved to be 0.047 and 0.104 cm^{-1} , with a recovery rate of 47-52%.

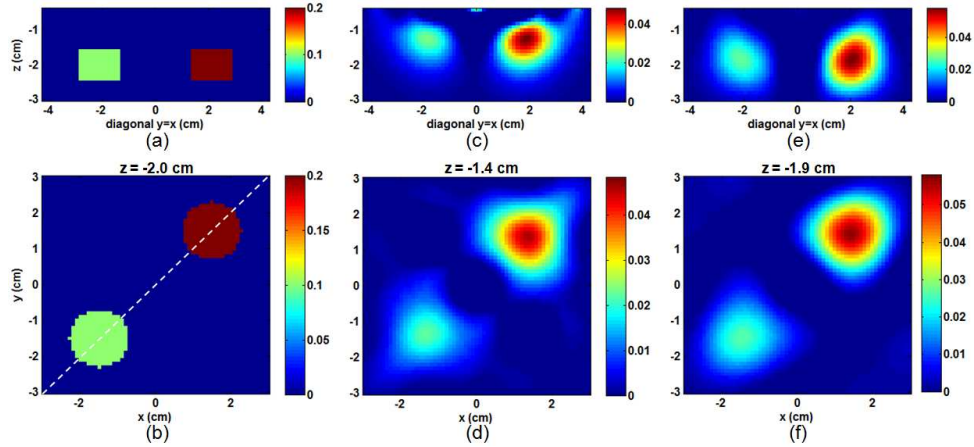


Fig. 3. For experiment II: Figs. 3(a), 3(c), 3(e) are depth cross sections along the diagonal plane at $y = x$, which is marked by the dash line in (b), of the (a) actual and reconstructed absorbers (c) without and (e) with depth compensation being utilized. Figures 3(b), 3(d), 3(f) are lateral cross sections in the x-y plane of the (b) actual and recovered absorbers (d) without and (f) with depth compensation applied, respectively.

Experiment III: Fig. 4(a) shows a depth cross section (along diagonal plane at $y = x$) of the two simulated absorbers. The actual absorbers are located at $z = -2.2$ and -1.8 cm with the same $\Delta\mu_a$ value of 0.2 cm^{-1} . Correspondingly, Fig. 4(b) shows the depth cross section of the reconstructed absorber without using depth compensation. Both absorbers are untruthfully projected to $z = -1.4$ cm, regardless of their actual depths. Without either depth compensation or ROI-based spatial prior applied, the recovered $\Delta\mu_{a_max}$ values for the two absorbers are 0.024 and 0.053 cm^{-1} , largely different from one another and from the single true value (0.3 cm^{-1}). After two separate ROIs are identified in two sub regions, using the same method as Experiment II, the determined $\Delta\mu_{a_ROI}$ values are 0.020 and 0.055 cm^{-1} for the respective absorbers, as low and wrong as the $\Delta\mu_{a_max}$ values.

In contrast, Fig. 4(c) shows the depth cross section of the reconstructed DOT image when depth compensation is applied. Two absorbers are projected to $z = -2.1$ and -1.7 cm, being very close to their actual depths. With depth compensation but without spatial prior, the $\Delta\mu_{a_max}$ values for the two absorbers are 0.020 and 0.052 cm^{-1} . Then after two spatial priors are applied in two sub regions, the recovered $\Delta\mu_{a_ROI}$ values of the respective absorbers are improved to be 0.075 and 0.091 cm^{-1} , with recovery rate of 38-46% of the actual values. It is also noteworthy that the $\Delta\mu_{a_ROI}$ values become less different between the two absorbers.

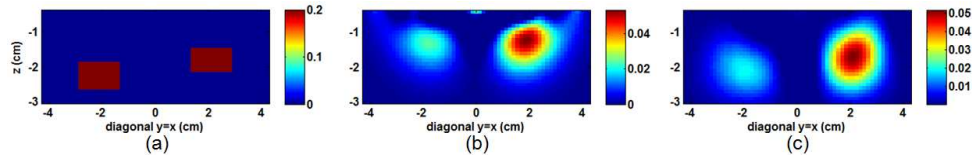


Fig. 4. For experiment III: a depth cross section along the diagonal plane at $y = x$ of the (a) actual absorbers, (b) reconstructed DOT image without depth compensation, and (c) reconstructed DOT image with depth compensation.

Overall, the recovered absorption perturbations from experiments I to III are listed in Table 1, where $\Delta\mu_a$ is the actual value of absorption perturbation, $\Delta\mu_{a_max}$ and $\Delta\mu_{a_ROI}$ are the recovered values without and with the use of ROI-based spatial prior, respectively.

Table 1. Actual absorption perturbation, $\Delta\mu_a$, maximum absorption perturbation recovered without ROI, $\Delta\mu_{a_max}$, and absorption perturbation recovered with ROI, $\Delta\mu_{a_ROI}$, for each absorber in experiments I to III. Unit: cm^{-1}

Experiment	Absorber	$\Delta\mu_a$	DOT without depth compensation		DOT with depth compensation	
			$\Delta\mu_{a_max}$	$\Delta\mu_{a_ROI}$	$\Delta\mu_{a_max}$	$\Delta\mu_{a_ROI}$
I	1	0.2	0.059	0.059	0.070	0.122
II	1	0.1	0.024	0.022	0.027	0.047
	2	0.2	0.048	0.048	0.058	0.104
II	1	0.2	0.024	0.020	0.020	0.075
	2	0.2	0.053	0.055	0.052	0.091

The results seen in all three simulated experiments demonstrate clearly that the depth-compensated reconstruction with a spatial prior is critically useful to recover the absorption perturbation. In contrast, a spatial prior without depth-compensated reconstruction brings little improvement for the recovery of absorption perturbation, which is the case of conventional DOT imaging. Therefore, the success of our approach to improve the quantification in DOT requires the combination of the spatial prior with depth-compensated reconstruction.

3.2 Noise suppression

Given the setup in Experiment I, the simulated data sets with and without 1% random noise are used to illustrate the results in this sub-section.

Noise interference: Figs. 5(a) and 5(b) show the reconstructed depths of the absorber at variable α and γ values, using the data without and with noise, respectively. It is clearly seen in Fig. 5(b) that if 1% random noise is added in the data, for the two reconstruction algorithms with and without depth compensation, the recovered depths of absorber are stable/consistent only when α is 10^{-3} and bigger (marked by the dashed line in that figure). Thus, two reconstruction algorithms have approximately same sensitivity to noise.

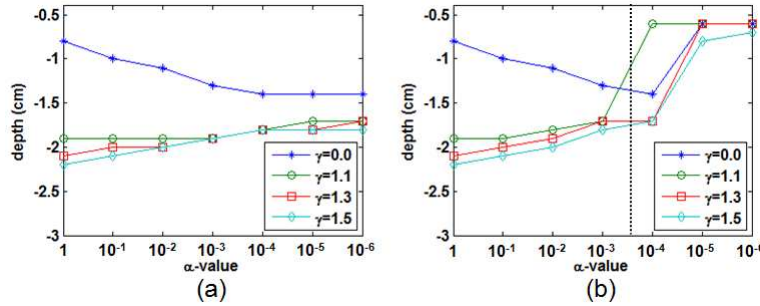


Fig. 5. Reconstructed depths of the absorber, using the setup of Experiment I in Fig. 1(a), with variable α and γ values when data were (a) noise-free and (b) with 1% random noise. Conventional DOT without depth compensation is equivalent to $\gamma = 0$. In (b) the reconstructed depths become divergent roughly after $\alpha = 10^{-3}$, which is attributed to the 1% random noise. The expected depth of the absorber is at $z = -2$ cm.

Depth localization: Figs. 5(a) and 5(b) also illuminate how the depth localization is affected when both α and γ vary. For all α values which can stabilize the inverse solutions (between 1 and 10^{-6} for noise-free data, and between 1 and 10^{-3} for data with 1% random noise), with the use of conventional DOT without depth compensation ($\gamma = 0$), a smaller α value results in a better accuracy in depth, approaching to, but never reaching the actual depth at $z = -2$ cm. When a big α -value is used (which in principle should be used for more noisy data), the reconstructed image without depth compensation has a very significant depth error as the absorber is untruthfully projected toward the surface. When depth-compensated reconstruction is applied, the reconstructed depth of absorber is relatively stable, within ± 3 mm of its actual depth, rather independent of either α or γ (between 1.1 and 1.5). The overall results in Fig. 5 demonstrate that when depth compensation is used in DOT reconstruction, any value of γ in the range of 1.1 to 1.5 is able to provide reliable depth localization with a 3-mm possible deviation for data at variable noise levels, even at a high noise level which may mandate the regularization parameter α to be a large value of 0.1 or 1.

Quantification: Using the data set with 1% random noise, values of $\Delta\mu_{a_max}$ and $\Delta\mu_{a_ROI}$ of the absorber were also quantified at variable α and γ values. Figures 6(a) and 6(b) show the quantified $\Delta\mu_{a_max}$ and $\Delta\mu_{a_ROI}$ values of the absorber within $\alpha \geq 10^{-3}$ since the reconstruction becomes unstable when $\alpha < 10^{-3}$ [see Fig. 5(b)]. Note that each of these two figures includes the data obtained both without ($\gamma = 0$) and with depth compensation. In addition, Fig. 6(c) shows the volumes of the identified ROI, V_{ROI} (in cm^3), for respective cases and within $\alpha \geq 10^{-3}$. Without the ROI-based spatial prior, Fig. 6(a) plots $\Delta\mu_{a_max}$ values at four different γ values, none of which can recover the actual absorption perturbation in a reasonable range. The best recovery rate is $\sim 28\%$ when $\alpha = 10^{-3}$.

On the other hand, when both depth-compensated reconstruction and ROI-based spatial prior are used for the respective cases, Fig. 6(b) shows that the reconstructed values of $\Delta\mu_{a_ROI}$ are in a range of 25-64% recovery with respect to the actual value of the absorber ($\Delta\mu_a = 0.2 \text{ cm}^{-1}$) while both α and γ values are varied. Specifically, a smaller α value seems to lead to an improved $\Delta\mu_{a_ROI}$, as expected. At $\alpha = 10^{-3}$, for example, the $\Delta\mu_{a_ROI}$ values are 52% and 62% recovered with $\gamma = 1.1$ and 1.5, respectively. In contrast, $\Delta\mu_{a_ROI}$ shows a mere 5-27% recovery rate when depth-compensated reconstruction is not used ($\gamma = 0$), even though the ROI-based spatial prior are formed appropriately.

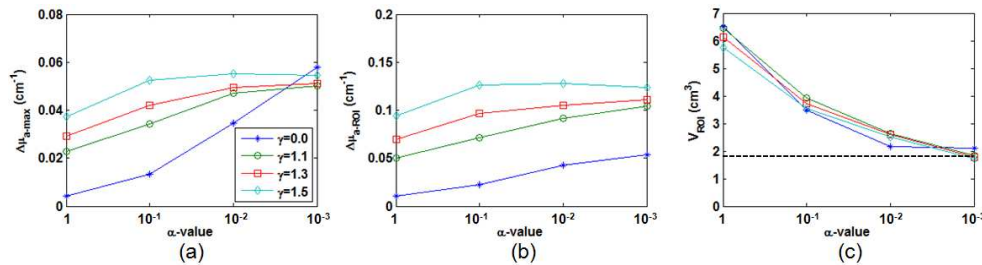


Fig. 6. Quantified (a) $\Delta\mu_{a,max}$, (b) $\Delta\mu_{a,ROI}$ and (c) V_{ROI} values of the absorber, with the given setup in Experiment I, when α and γ values are varied. The expected $\Delta\mu_a$ value is 0.2 cm^{-1} . The expected volume of the absorber is 1.7 cm^3 . Conventional DOT without depth compensation is equivalent to $\gamma = 0$.

Furthermore, Fig. 6(c) shows the dependence of ROI volumes, V_{ROI} , on α for all cases (without and with depth compensation in reconstruction), illustrating a decreasing pattern as α values become smaller. This trend can account for the increasing trend in $\Delta\mu_{a,ROI}$ with reduced α value, as seen in Fig. 6(b). At $\alpha = 10^{-3}$, the values of V_{ROI} approach the actual volume of the absorber, which is marked by the dash line in Fig. 6(c), for variable γ values.

4. Discussion and conclusion

Accurate quantification of a local absorption perturbation has been a major challenge in the field of DOT for functional brain imaging. When multi-channel data are collected in DOT to reconstruct an image of the brain activation, the accuracy in quantification relies greatly on the accuracy in localization of the reconstructed object, or the activated regional volume in the brain, particularly along the direction of depth. Unfortunately, the conventional reconstruction algorithm in DOT is not able to compensate the severe attenuation in sensitivity with increased depth, resulting in a significant depth error.

An algorithmic depth compensation has been developed and demonstrated to be able to accurately localize the absorption perturbation in our previous reports [5,6]. Consequently, this algorithm has a potential to improve the accuracy in quantification. In this paper, we have presented an approach based on the depth compensation algorithm that can be used to improve the quantification of absorption perturbation. The fundamental idea of this approach is to generate a spatial prior by half-maximum thresholding so that the reconstructed image can recover the object closely to its actual size and location. Three simulative experiments have been conducted to validate the approach using absorbers with variable absorption contrasts as well as at different locations and depths. When the depth compensation algorithm is utilized without a spatial prior, the reconstructed maximum values, $\Delta\mu_{a,max}$, of absorption perturbations in each experiment are comparable to those obtained without using any depth compensation. But, none of them can recover well the true values of absorption perturbation. Then after defining an appropriate ROI by half-maximum thresholding in the reconstructed image with depth compensation, the accuracy in quantification is improved greatly in each of the three experiments. More significant improvement has been observed for deeper absorbers, as demonstrated in experiment III (Fig. 4). The results given throughout all three experiments are reasonable and expected since the spatial priors with depth-compensated reconstruction are relatively close to the actual locations and sizes of the absorber(s) in each experiment. Since the spatial prior utilized in this approach also depends on the spatial resolution of reconstructed image, we expect that the accuracy of quantification using this approach may vary somewhat for different probe geometries. Such expectation needs to be studied in future.

In addition to the simulative experiments described above, we have also conducted an Intralipid phantom experiment to further validate our quantification approach. The setup for phantom experiment was the same as simulative experiment I, which is shown in Fig. 1(a). The optical properties of the phantom were measured with a dual-channel tissue oximeter (Model 96208, ISS INC., Champaign, IL) at 750 and 830 nm. The data was acquired with a high-density DOT system at 750 and 850 nm [13], using the probe geometry shown in

Fig. 1(a). Since the tissue oximeter and DOT system shared the same wavelength at 750 nm, we analyzed the data at this wavelength only. Specifically, the phantom had absorption and reduced scattering coefficients of 0.08 and 11.1 cm⁻¹ at 750 nm, respectively. The cylindrical absorber had approximately the same reduced scattering coefficient as the phantom, and a higher absorption coefficient of 0.23 cm⁻¹ at 750 nm. The absorber was embedded 2 cm into the phantom (i.e., $z = -2$ cm), which introduced an absorption perturbation of 0.15 cm⁻¹. Figures 7(a) and 7(b) show depth cross sections (y-z plane, $x = 0$) of the reconstructed DOT images without and with depth compensation, respectively. The cylindrical absorber is projected to $z = -1.4$ cm in reconstructed image without depth compensation and at $z = -1.7$ cm when depth compensation algorithm is applied. In both images, the $\Delta\mu_{a,max}$ values are much lower than the actual value (0.15 cm⁻¹). After a ROI is identified with half-maximum threshold to form a spatial prior, the $\Delta\mu_{a,ROI}$ value derived from the reconstructed image without depth compensation is 0.025 cm⁻¹, merely 17% of the actual value. The $\Delta\mu_{a,ROI}$ value derived from the reconstructed image with depth compensation is improved to 0.042 cm⁻¹, about 28% of the actual value. Within the experimental error, the depth-compensated reconstruction with the spatial prior significantly improves the recovery rate of absorption perturbation, although it is still far from being ideal.

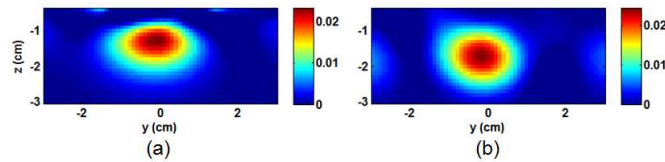


Fig. 7. For phantom experiment, a depth cross section (y-z plane, $x = 0$) of the reconstructed DOT image (a) without depth compensation, and (b) with depth compensation. The cylindrical absorber was located at $z = -2.0$ cm which had an actual $\Delta\mu_a$ of 0.15 cm⁻¹.

The noise suppression also plays a role in DOT reconstruction, with and without depth compensation, which affects the size and location of object in reconstructed image. Using the setup in Experiment I as an example, a comprehensive comparison on the noise suppression has been conducted to investigate the (1) deviations of the reconstructed object depths and (2) recovery rates of absorption perturbations that were derived from reconstructed images without and with depth compensation while values of α and γ were varied. The reconstruction outputs from the data without and with 1% random noise illustrate that the two reconstruction algorithms, i.e., reconstruction with and without depth compensation, have approximately same sensitivity to noise. For all α values which can stabilize the inverse solutions, however, the recovered DOT images without applying depth compensation cannot exhibit the correct depth ($z = -2$ cm) of the absorber, regardless of any α value used. On the other hand, if depth compensation is employed, the reconstructed depths are much closer to the expected value ($z = -2$ cm) without any restriction in α values for noise-free data and with α larger than 10^{-3} for the data having 1% random noise.

More importantly, the investigation on inter-parameter effects between α and γ on depth localization reveals that conventional DOT reconstruction is more restricted by the noise suppression procedure. For example, when a big α value is employed for more noisy data, conventional DOT algorithm ($\gamma = 0$) has a very significant depth error. On the other hand, when depth compensation algorithm is combined in the DOT reconstruction, the recovered depth of the absorber is relatively stable across a broad range of α values when an optimal γ range is selected (between 1.1 and 1.5). It is a strong support that the depth compensation algorithm can provide reliable and accurate depth localization for data at variable noise levels. This finding is practically important with the consideration of the physiological noises to be encountered during *in vivo* human brain measurements [2]. Furthermore, the accurate localization of the absorption perturbation based on the depth compensation algorithm leads to appropriate selection of ROIs, which consequently improves the accuracy in quantification that cannot be achieved by the conventional DOT reconstruction without depth compensation.

Overall, in this study, we have presented an approach based on our recently developed depth compensation algorithm to quantify the absorption perturbation in DOT with reasonable recovery rates. By applying this approach, quantification of absorption perturbation can be recovered with a best rate of 64% in simulative experiments. Moreover, the comprehensive comparison on the noise suppression demonstrates that the combination of the depth compensation algorithm with ROI-based spatial prior offers a reliable and accurate depth localization and improved quantification in DOT at variable noise levels. Moreover, while our approach targets primarily on the application of functional brain imaging, the improvements in quantification potentially can be extended to other applications of DOT, e.g., the detection of cancer where reflectance geometry is used.

Acknowledgement

This work was supported in part by National Institute of Health (NIH) funding from NINDS (4R33NS052850-03).